A narrow, mid-mantle plume below southern Africa

Daoyuan Sun,[1,2] Don Helmberger,[1] and Michael Gurnis[1]

Received 29 December 2009; revised 16 March 2010; accepted 29 March 2010; published 4 May 2010.

[1] New waveform tomographic evidence displays a narrow plume-like feature emitting from the top of the large African low-velocity structure in the lower mantle. A detailed SKS wavefield is assembled for a segment along the structure's southern edge by combining multiple events recorded by a seismic array in the Kaapvaal region of southern Africa. With a new processing technique that emphases multi-pathing, we locate a relatively jagged, sloping wall 1000 km high with low velocities near it's basal edge. Forward modeling indicates that the plume's diameter is less than 150 km and consistent with an isochemical, low-viscosity plume conduit. **Citation:** Sun, D., D. Helmberger, and M. Gurnis (2010), A narrow, mid-mantle plume below southern Africa, *Geophys. Res. Lett.*, *37*, L09302, doi:10.1029/2009GL042339.

1. Introduction

[2] The resolution of global tomographic models, which have increased through additional data while accounting for the finite frequency of seismic waves, have provided more details on possible plumes in the lower and upper mantle [*Montelli et al.*, 2004, 2006]. Although some of these features have small cylindrical forms, most are broad, especially at the base of the mantle, where they are commonly referred to as Large Low Shear Velocity Provinces (LLSVP, Figure 1). Images beneath the mid-Pacific and South Africa show considerable differences but the change of scale from about 1000 km in the lower mantle to a few hundred in the mid-mantle is a common feature of nearly all seismic inversions. The average δV_S for the lower portion of the LLSVP is about −3%, whereas δV_P is much smaller [*Masters et al.*, 2000; *Tan and Gurnis*, 2005; 2007]. They may also have lateral density perturbations of by a few percent [*Ishii and Tromp*, 1999; *Resovsky and Trampert*, 2003].

[3] Models of thermo-chemical convection are consistent with these observations [*Davaille*, 1999; *Garnero and McNamara*, 2008; *McNamara and Zhong*, 2004, 2005; *Tackley*, 2002]. A composition-dependent compressibility model with a high bulk modulus (Figure 1b) is constructed to satisfy the inverse correlation between shear velocity and bulk sound speed found in tomographic inversions [*Masters et al.*, 2000] (Figure S1), while simultaneously giving sharp vertical sides with the apparent long term stability of the African LLSVP [*Tan and Gurnis*, 2005, 2007]. A narrow plume emerges from the top with a small amount of entrainment of the high bulk modulus mantle. By embedding this dynamic model into a radial seismic reference model PREM [*Dziewonski and Anderson*, 1981], we showed that travel times computed synthetically match observed anomalies [*Sun et al.*, 2007]. In particular, the model predicts about a 6s jump in SKS travel times when crossing the edges of the African LLSVP (Figures S2a–S2b).

[4] The sharpness of the edges is obvious in the seismic waveforms (Figure 2a). Although waveforms are generally displayed as record sections plotted with increasing distance, vertical structures become more obvious in azimuthal sections. For the African section, the northernmost stations display simple but delayed pulses (red zone) while the southern stations have PREM-like times (blue zone). The various ray paths (Figure 2c) indicate that the crossing into the relatively slow velocities is associated with extra travel time. Complex seismograms occur near the change in travel time (212° in Figure 2a) and hence near a velocity boundary. Presumably, the complexity is caused by multi-pathing where we observed two arrivals, one from outside (arriving early) and one from the inside the low velocity structure (arriving late). These observations are similar to synthetics for a wall-crossing (Figures S3 and S4). Moreover, analytic synthetics suggest that the complex waveforms can be fit to first-order with two pulses with one simply delayed by the slower path [*Sun et al.*, 2009]. In the next section we will discuss Figure 2b and a new approach of extracting parameters from complex waveforms.

[5] In this paper we will review parameterizing complexity, followed by a section on processing multiple events to form a composite picture of observed features. We then use this data to construct a model and demonstrate that synthetics from this model fit the same complexity pattern observed.

2. Method

[6] In this section, we introduce the Multi-Path Detector (MPD) analysis that exploits the complexity and resolves sharp structures, see Text S1 of the auxiliary material for more details.[3] We assume that the splitting is controlled by travel time differentials between arrivals, which can be captured by two-dimensional arrays. We first determine an Empirical Source Function, ESF(t), which is the simplest waveform in the array. Next, we generate a synthetic for a reference model using this S(t) = ESF(t)/2 by assuming each seismogram can be modeled by summing S(t) + S(t + Δ_{LR}). We define Δ_{LR} as the time separation, which refers to the lag of the right half of the Fresnel zone relative to the left, or split time. The travel time of the composite (Figure 2b) relative to the reference model is defined as Δ_T. The Δ_T's are displayed in Figure 2c and the Δ_{LR}'s are given in Figure 2d. Thus, if we neglect diffraction features as indi-

[1]Seismological Laboratory, California Institute of Technology, Pasadena, California, USA.
[2]Now at Department of Terrestrial Magnetism, Carnegie Institution of Washington, Washington, DC, USA.

0094-8276/10/2009GL042339

[3]Auxiliary materials are available in the HTML. doi:10.1029/2009GL042339.

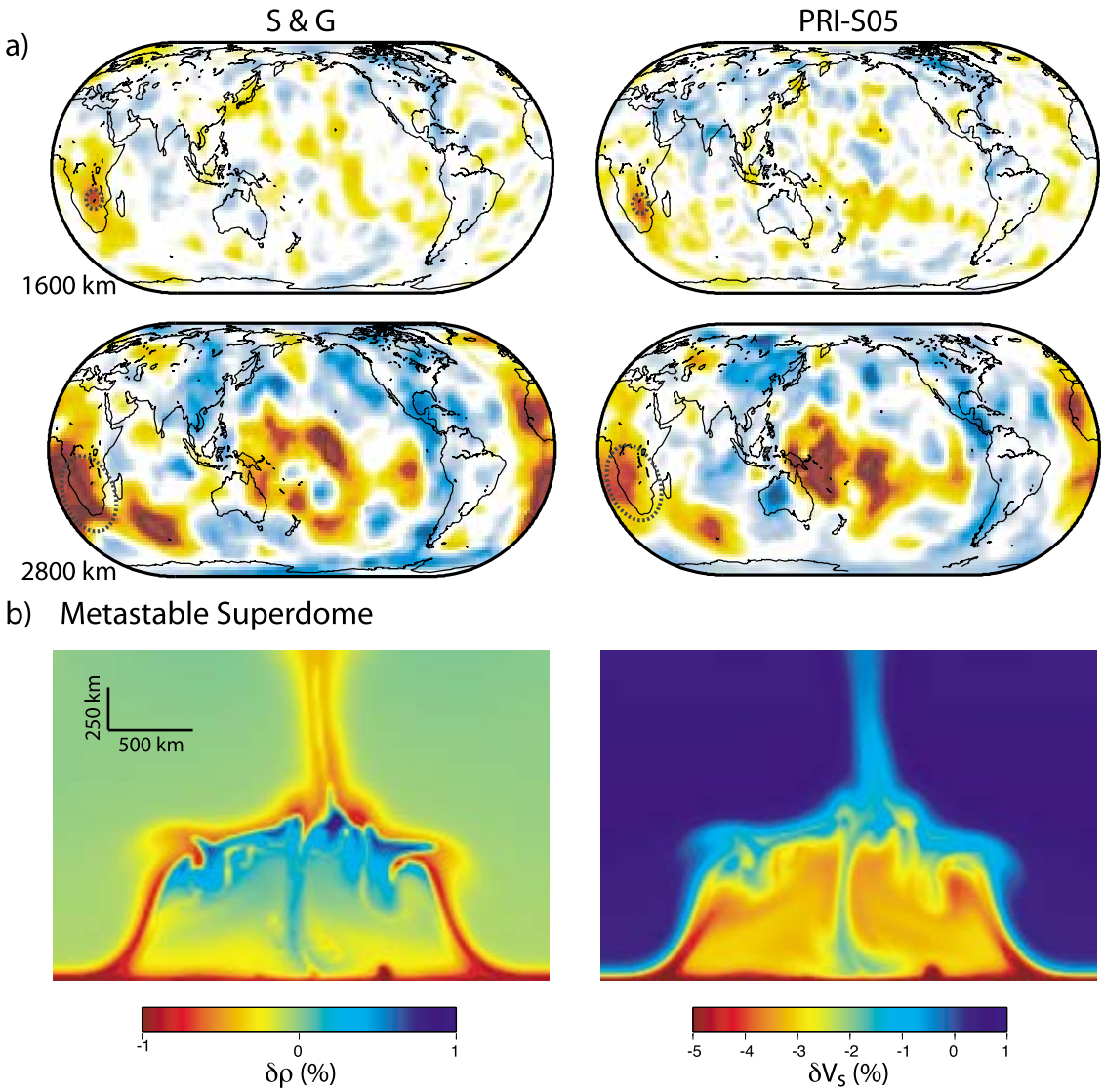

Figure 1. A comparison of global tomographic images (a) at the lower mantle [after *Montelli et al.*, 2006] with a predicted cross-section (b) of seismic properties from a meta-stable thermo-chemical structure. The anomalous material has a larger bulk modulus (6% above the ambient) and higher density (2.25%). The S&G shear velocity (left) variations (±3%, blue and red) are from *Grand* [2002] and the PRI-S05 shear velocity (right) is from *Montelli et al.* [2006]. The agreement between these two models is remarkable considering the complete independence of data and methodology used [*Helmberger and Ni*, 2005]. We interpret the broad base in the data at the CMB (Africa) to be a large-scale chemical pile and the upper small dimension feature to be a plume.

cated by the dotted line in Figure 2a, we will distinguish between in-plane vs. out-of-plane multi-pathing effects. The usefulness of this measure is discussed by *Sun et al.* [2009] based on array analysis of synthetics. The gradient in Δ_{LR} constructed from the array forms a vector indicating a diffraction pattern as in optics. Note that the vector points to the structural edge causing the multi-pathing. In this case, the vectors are not purely in the azimuthal direction suggesting that there is some radial or depth sensitivity as well. However, the boundary is well defined where the gradient changes sign and occurs along the ray path specified by the heavy dash line in Figure 2d, indicating a sharp change in velocity. The data analysis given in Figure 2 applies to the southern edge of the LLSVP. A similar pattern of multi-pathing occurs along the northern boundary of this structure (Figure S5).

[7] The height of the structure remains an issue but some direct evidence is available [*Ritsema et al.*, 1998]. Although the geometry for sources and receivers is lacking for sampling the top of the LLSVP with direct S, the phase SS can be used as proposed by *Ni et al.* [2005] where one leg of the SS phase samples along the top of the LLSVP. The roughness of the upper structure also causes multi-pathing as given in Figure S6 for the SS phase. In addition some secondary arrivals following Sd have timing appropriate for scattered waves near the top of the structure (Figure S5).

3. Results and Model

[8] Although profiles of data such as Figures 2 and S5 are sufficient to establish sharpness, they are not ideal for detailed study because of lack of knowledge about the

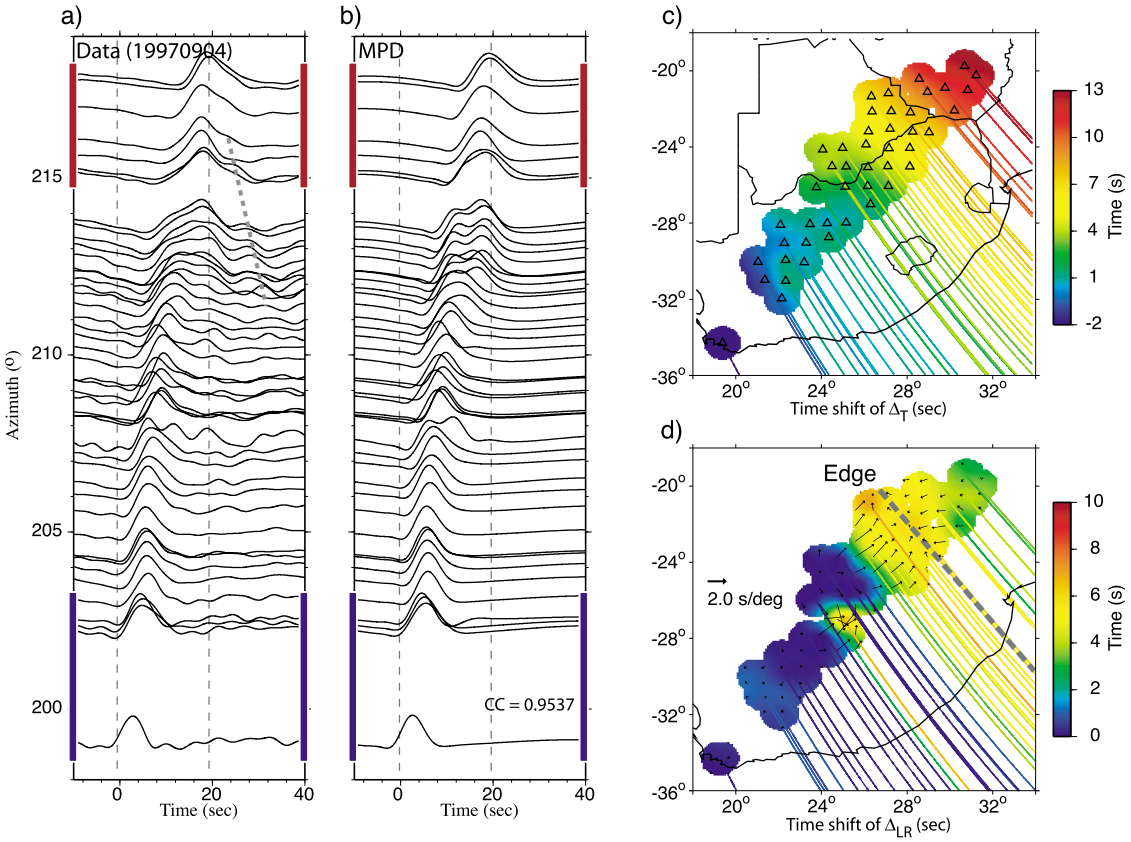

Figure 2. (a) S-waveform observations are plotted as a function of azimuth along with (b-d) Multi-Path Detector (MPD) simulations and timing delays. The data is from the Fiji-Tonga region with geometry given in Figure S2c. The ray paths as they enter the array are color-coded indicating their delays in Figure 2c and splitting in Figure 2d. Note that the waveforms are about 10s late for northernmost paths compared to southern paths. Near about 212°, the waveforms indicate strong multi-pathing with separations more than 6s. We find the wall crossing where the gradient changes signs occur along the ray path specified by the heavy dash line in Figure 2d.

structure beneath the Indian Ocean [*Wang and Wen*, 2007]. A better geometry is provided by the SKS paths sampling the mostly 2D structure from the west over a 10° by 20° region forming a relatively dense sample (Figure S2). Although these small crustal events along the East Pacific-Rise (EPR) have complicated wave trains they remain stable in the MPD. The four EPR events were processed in this manner (Figure S7).

[9] The combined Δ_T delays are plotted with respect to CMB exit points (Figure 3a), normalized by a constant time shift for all stations per event. Such baseline shifts are common because of uncertainties in the event origin time and location. However, the relative timing among the stations is maintained. Delays of up to 6s are obtained with the four events producing compatible results. The paths overlay with some crossing paths indicated by the arrows in Figure 3a. The splitting analysis is summarized in Figure 3b where a serious distortion of waveforms occurs along the southern edge (−45°N15°E). Unfortunately, the details are unclear because of the noisy complex arrivals as well as limitations in data coverage. This location has been studied previously with ScS-S analysis where they suggest a strong ultra low velocity-zone [*Simmons and Grand*, 2002; *Wang and Wen*, 2007; *Wen*, 2001], which may correlated with the slow velocity edge structure in the high bulk modulus model (Figure 1b).

[10] Because of SKS relatively steep ray paths, their spatial pattern proves highly effective in mapping horizontal structure. Thus, we will assume that these patterns in Figure 3a are controlled entirely by velocity variation along these SKS paths. Furthermore, we will assume that paths inside the structure encounter a −3% reduction in shear velocity as in metastable plume model [*Sun et al.*, 2007]. This is a simplification but allows a structural image to be formed by performing a SKS tomographic projection on Figure 3a upward to define the height. A plume feature is added to the 2D profile based on the circular red pattern (Figure 3b) located along the upper dotted line near the top of the dome to fit the Δ_{LR} delay. A 2D section of our preferred model crossing through the plume is given in Figure 3d, where we have assumed the velocity reduction inside the plume is 1.5%. Its height trade-offs with this value because only the timing delay Δ_{LR} ~ 3s is defined by the data. We assumed this value to be compatible with estimates obtained by the high bulk modulus model given in Figure 1b.

[11] We constructed synthetics for this 3D model and performed the same MPD analysis on these simulations with results given in Figures 3e–3f. The simulated pattern is smoother because it assumes a uniform source while the composite contains multiple events. Nevertheless, the patterns match along with the same circular Δ_{LR} patch at the tip of South Africa. This small patch was constructed from a

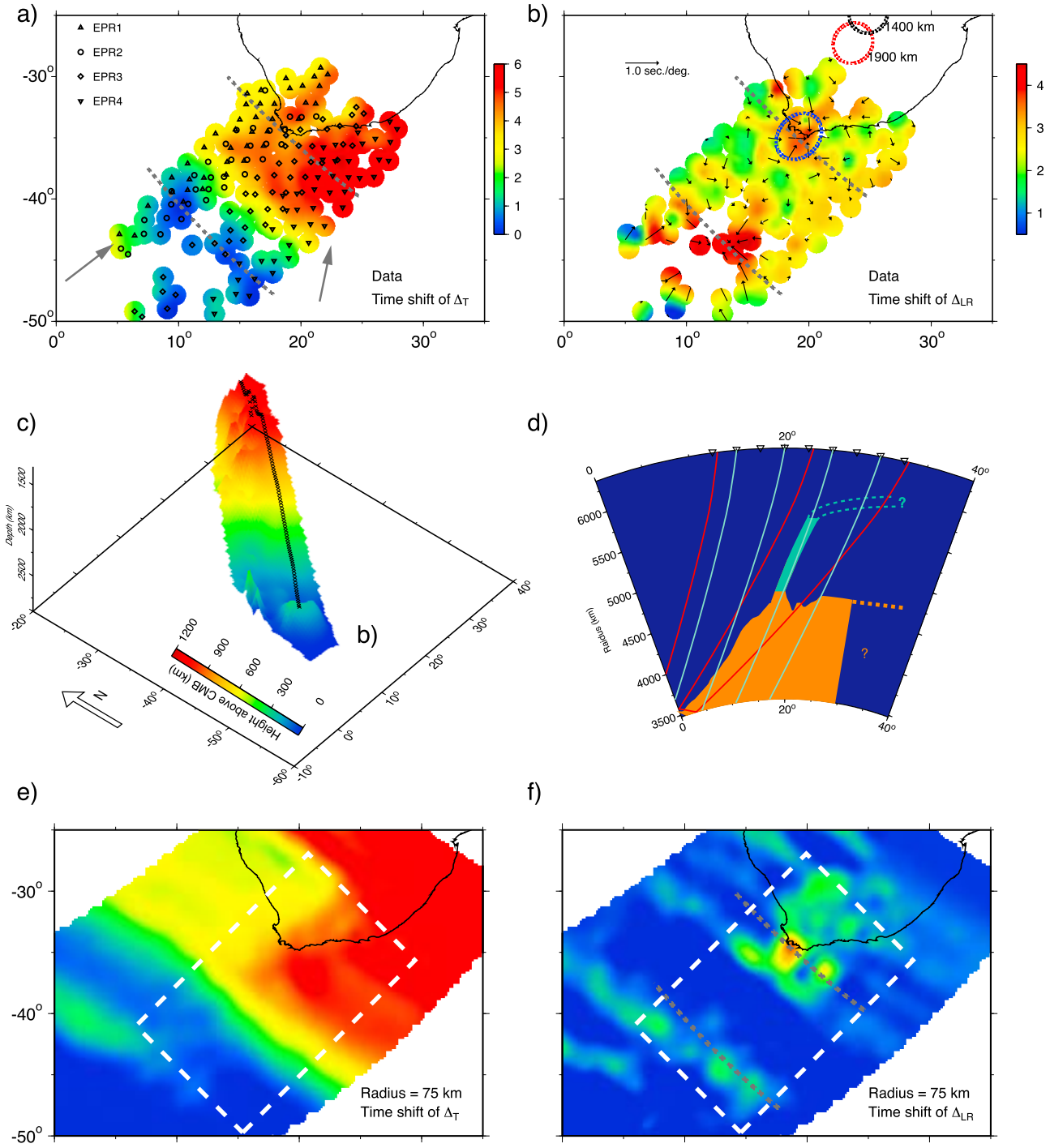

Figure 3. Composite waveform information from four EPR events compared to corresponding MPD analysis from various plume models. (a) The delay Δ_T and (b) differential values Δ_{LR} are migrated down to the CMB and plotted in map form for various events. Two heavy lines are added in Figure 3b to indicate the bottom and top of the LLSVP where the SKS travel time delays climb to 6 s. Note the blue circle of vectors near the South tip of Africa with radius of 1°. (c) A 3D image is displayed. (d) A 2D cross-section sampling the plume is displayed idealized with a uniform reduction of 3% inside the LLSVP (orange), a 1.5% drop inside the plume (green), which extends about 1000 km into the top part of the lower mantle. Although the shape of the top and fine-scale features displayed in Figure 3d lack resolution with current observations, the model looks very much like the models presented in Figure 1a with a broad base and a pipe-like feature extending upward towards the north. (e and f) A simulation is displayed with this circular shaped plume (Figure 3d) emitting from the top of the LLSVP. As the radius of the plume grows, a small zone of delayed Δ_T occurs because the wavefield begins to resolve the interior directly which is not in the observations (Figure S8). The small circle indicating the plume position at the CMB in Figure 3a migrates to the northwest for mid-mantle positions displayed at depths of 1900 km (red circle) and 1400 km (black circle).

radius of 75 km, see Figures S8 and S9 for synthetics at larger radii and MPD analysis. The models with larger radius do not fit the data.

[12] Note that this pattern is back projected from the surface along SKS paths to the CMB. Thus, the pattern shifts northeastward for shallower mantle depths as indicated by the circles in Δ_{LR} of Figure 3a. Both the S-velocity of *Grand* [2002] and of *Montelli et al*. [2006] predict this behavior although the P-velocity results suggest some bifurcation at shallower depths [*Montelli et al.*, 2006]. Our results are in contrast with *Montelli et al.* [2006] from finite frequency tomography, suggesting a range of widths from 200 to 800 km. Large widths are consistent with only a small viscosity between the plume and mantle rising in the plume [*Olson and Singer*, 1985] or thermo-chemical structures, both favor wide-blunt plumes.

[13] Two dynamic models have been proposed to explain the LLSVP's, the high bulk modulus model presented here [*Tan and Gurnis*, 2005, 2007] and the chemical pile model [*McNamara and Zhong*, 2004, 2005]. The former has steeper sides (~70°) while the latter one has gentle slopes (~30°). Our results are in the middle (50° ~ 60°). Both MPD images (Figures 3c–3d) and multi-pathing in SS phase suggest a rough top of the LLSVP, which is more profound in high bulk modulus model. In this report, we only covered the southern edge and more data are needed to complete the entire image, which will greatly help to define the dynamics of the system.

[14] In summary, we have discovered direct seismic evidence for the existence of a narrow pipe-like structure emanating from the top of the large African slow structure. However, we still need to refine images passing through the upper mantle transition zone and the 3D nature of these complex conduits. In short, a great deal of geosciences is needed to understand this new class of large-scale small-scale interactions and how heat travels from the CMB to the surface.

[15] **Acknowledgments.** The authors would like to thank the Editor Michael Wysession, Allen McNamara, and an anonymous reviewer for their comments. This work was supported by the National Science Foundation, grant MCG.00021-1-NSF.CSEDIFINE and contribution 10040 of the Division of Geological and Planetary Science, California Institute of Technology.

References

Davaille, A. (1999), Simultaneous generation of hotspots and superswells by convection in a heterogenous planetary mantle, *Nature*, *402*(6763), 756–760, doi:10.1038/45461.

Dziewonski, A. M., and D. L. Anderson (1981), Preliminary reference Earth model, *Phys. Earth Planet. Inter.*, *25*, 297–356, doi:10.1016/0031-9201(81)90046-7.

Garnero, E. J., and A. K. McNamara (2008), Structure and dynamics of Earth's lower mantle, *Science*, *320*(5876), 626–628, doi:10.1126/science.1148028.

Grand, S. P. (2002), Mantle shear-wave tomography and the fate of subducted slabs, *Philos. Trans. R. Soc. London A*, *360*(1800), 2475–2491.

Helmberger, D. V., and S. Ni (2005), Seismic modeling constraints on the South African super plume, in *Earth's Deep Mantle: Structure, Composition, and Evolution*, *Geophys. Monogr. Ser*, vol. 160, edited by R. D. van der Hilst et al., pp. 63–81, AGU, Washington, D. C.

Ishii, M., and J. Tromp (1999), Normal-mode and free-air gravity constraints on lateral variations in velocity and density of Earth's mantle, *Science*, *285*(5431), 1231–1236, doi:10.1126/science.285.5431.1231.

Masters, G., G. Laske, H. Bolton, and A. M. Dziewonski (2000), The relative behavior of shear velocity, bulk sound speed, and compressional velocity in the mantle: Implications for chemical and thermal structure, in *Earth's Deep Interior: Mineral Physics and Tomography From the Atomic to the Global Scale*, *Geophys. Monogr. Ser*, vol. 117, edited by S. Karato et al., pp. 63–87, AGU, Washington, D. C.

McNamara, A. K., and S. Zhong (2004), Thermochemical structures within a spherical mantle: Superplumes or piles?, *J. Geophys. Res.*, *109*, B07402, doi:10.1029/2003JB002847.

McNamara, A. K., and S. Zhong (2005), Thermochemical structures beneath Africa and the Pacific Ocean, *Nature*, *437*(7062), 1136–1139, doi:10.1038/nature04066.

Montelli, R., G. Nolet, F. A. Dahlen, G. Masters, E. R. Engdahl, and S. H. Hung (2004), Finite-frequency tomography reveals a variety of plumes in the mantle, *Science*, *303*(5656), 338–343, doi:10.1126/science.1092485.

Montelli, R., G. Nolet, F. A. Dahlen, and G. Masters (2006), A catalogue of deep mantle plumes: New results from finite-frequency tomography, *Geochem. Geophys. Geosyst.*, *7*, Q11007, doi:10.1029/2006GC001248.

Ni, S. D., D. V. Helmberger, and J. Tromp (2005), Three-dimensional structure of the African superplume from waveform modelling, *Geophys. J. Int.*, *161*(2), 283–294, doi:10.1111/j.1365-246X.2005.02508.x.

Olson, P., and H. Singer (1985), Creeping plumes, *J. Fluid Mech.*, *158*, 511–531, doi:10.1017/S0022112085002749.

Resovsky, J., and J. Trampert (2003), Using probabilistic seismic tomography to test mantle velocity-density relationships, *Earth Planet. Sci. Lett.*, *215*, 121–134, doi:10.1016/S0012-821X(03)00436-9.

Ritsema, J., S. Ni, D. V. Helmberger, and H. P. Crotwell (1998), Anomalous shear velocity reductions and gradients in the lower mantle beneath Africa, *Geophys. Res. Lett.*, *25*, 4245–4248, doi:10.1029/1998GL900127.

Simmons, N. A., and S. P. Grand (2002), Partial melting in the deepest mantle, *Geophys. Res. Lett.*, *29*(11), 1552, doi:10.1029/2001GL013716.

Sun, D., E. Tan, D. V. Helmberger, and M. Gurnis (2007), Seismological support for the metastable superplume model, sharp features, and phase changes, within the lower mantle, *Proc. Natl. Acad. Sci. U. S. A.*, *104*(22), 9151–9155, doi:10.1073/pnas.0608160104.

Sun, D., D. Helmberger, S. Ni, and D. Bower (2009), Direct measures of lateral velocity variation in the deep Earth, *J. Geophys. Res.*, *114*, B05303, doi:10.1029/2008JB005873.

Tackley, P. J. (2002), Strong heterogeneity caused by deep mantle layering, *Geochem. Geophys. Geosyst.*, *3*(4), 1024, doi:10.1029/2001GC000167.

Tan, E., and M. Gurnis (2005), Metastable superplumes and mantle compressibility, *Geophys. Res. Lett.*, *32*, L20307, doi:10.1029/2005GL024190.

Tan, E., and M. Gurnis (2007), Compressible thermochemical convection and application to lower mantle structures, *J. Geophys. Res.*, *112*, B06304, doi:10.1029/2006JB004505.

Wang, Y., and L. Wen (2007), Geometry and P and S velocity structure of the "African Anomaly," *J. Geophys. Res.*, *112*, B05313, doi:10.1029/2006JB004483.

Wen, L. (2001), Seismic evidence for a rapidly varying compositional anomaly at the base of the Earth's mantle beneath the Indian Ocean, *Earth Planet. Sci. Lett.*, *194*, 83–95, doi:10.1016/S0012-821X(01)00550-7.

M. Gurnis and D. Helmberger, Seismological Laboratory, California Institute of Technology, Pasadena, CA 91125, USA.

D. Sun, Department of Terrestrial Magnetism, Carnegie Institution of Washington, Washington, DC 20015, USA. (dsun@dtm.ciw.edu)